Adiabatic flux insertion and growing of Laughlin states of cavity Rydberg polaritons

Peter A. Ivanov,[1,2] Fabian Letscher,[1,3] Jonathan Simon,[4] and Michael Fleischhauer[1]
[1]*Department of Physics and Research Center OPTIMAS, University of Kaiserslautern, Germany*
[2]*Department of Physics, St. Kliment Ohridski University of Sofia, James Bourchier 5 Boulevard, 1164 Sofia, Bulgaria*
[3]*Graduate School Materials Science in Mainz, Gottlieb-Daimler-Strasse 47, D-67663 Kaiserslautern, Germany*
[4]*Department of Physics and James Franck Insitute, University of Chicago, Chicago, Illinois 60637, USA*

(Received 27 March 2018; published 27 July 2018)

Recently, the creation of a strong magnetic field in a photonic cavity system has been demonstrated [N. Schine *et al.*, Nature (London) **534**, 671 (2016).]. Using this setup, we propose a scheme to adiabatically transfer flux quanta simultaneously to all cavity photons. The flux transfer is achieved using external light fields with orbital angular momentum and a near-resonant dense atomic medium as a mediator. Furthermore, by coupling the cavity fields to a Rydberg state, strong photon-photon interactions can be realized and fractional quantum Hall states can be prepared. To this end, a growing protocol is discussed consisting of a sequence of flux insertion and subsequent single-photon insertion. Specifically, we discuss the growing of the $\nu = 1/2$ bosonic Laughlin state. First we adiabatically insert two photonic flux quanta, creating a two-quasihole excitation, and second we refill the hole with a single photon using the strong photon-photon interactions.

DOI: 10.1103/PhysRevA.98.013847

I. INTRODUCTION

Over the last few years, there has been a remarkable progress in the experimental realization and study of topological models for photons [1,2]. Prominent examples are the creation of topological band structures in systems of coupled optical waveguides [3–5] and resonators [6]. Photonic systems have a number of potential advantages for spatially and time-resolved manipulation and detection of topological states. The ability to create strong interactions by coupling photons to Rydberg states [7–9], furthermore, offers the possibility to study many-body topological effects such as fractional quantum Hall physics or fractional Chern insulators [10–13]. As discussed in Refs. [12,13], lattice-free systems are preferable to obtain large interaction gaps. One way to realize an artificial magnetic field in a continuous system is to use the analogy between the Lorentz force of a magnetic field and a Coriolis force. This has been shown for ultracold neutral atoms by inducing a rotation of the atomic ensemble [14–17]. To transfer this idea to photons, however, requires either to make use of the drag effect of a rotating dispersive medium [18,19] or to enforce an effective rotation using nonplanar ring resonators. In the latter case, the nonplanar geometry induces a rotation of light rays about the optical axis on each round trip, as is shown in Fig. 1(a). This idea has recently been experimentally implemented and has led to the first demonstration of synthetic Landau levels (LLs) for photons [20,21]. Photons in such optical cavities provide an excellent experimental platform for the realization and observation of fractional quantum Hall physics due to the effective two-dimensional motion, the large intrinsic length scales, as well as the enhanced optical nonlinearity caused by mode confinement and cavity-enhanced interaction time [22].

In this paper, we discuss the preparation of the ground state of the photonic fractional quantum Hall (FQH) system, i.e., a photonic Laughlin (LN)-type state in the setup of Ref. [20], using the sequential growing technique suggested in [23,24]. The key ingredients of the scheme are the controlled insertion of single photons and the subsequent adiabatic insertion of an integer amount of magnetic flux quanta. Starting with a LN state, the flux insertion creates a quasihole excitation in the center of the system by transferring the right amount of angular momentum to the cavity photons. Subsequently, the hole is refilled by a single photon using a coherent laser field. Repeating the protocol, LN-type ground states can be prepared with high fidelity. Compared to the growing protocol presented in Ref. [25], our scheme has the advantage that quasiholes created by photon decay are continuously pumped to the periphery of the LN droplet. This allows one to prepare an almost defect-free quantum Hall liquid in the center.

To insert an integer number of flux quanta in a cavity setup, we propose an adiabatic method for transferring external orbital angular momentum (OAM) from classical light beams to the cavity photons by using an atomic ensemble as a mediator. Specifically, we show that an adiabatic transfer of OAM to the cavity photons can be achieved by using a stimulated Raman adiabatic passage (STIRAP) [26]. The transfer is facilitated by an infinite set of cavity dark states.

In order to realize a single-photon pump, the photonic cavity modes are coupled to a high-lying Rydberg state of an atomic medium under conditions of electromagnetically induced transparency (EIT) [7,27,28]. This results in a strong photon nonlinearity. Employing the resulting photon blockade, a single photon can be inserted into the system with high fidelity. Repeating a sequence of magnetic flux and subsequent single-photon insertion allows one to a grow the LN-type ground state.

The paper is organized as follows: In Sec. II, we briefly review the experimental setup of a photonic twisted cavity. In Sec. III, we discuss the adiabatic flux insertion technique in detail. Furthermore, we study imperfections which limit the

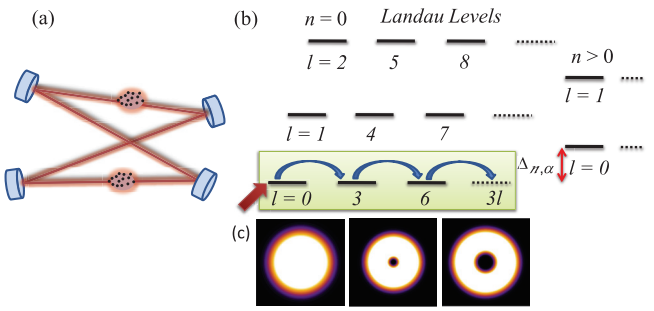

FIG. 1. (a) Nonplanar resonator consisting of four mirrors creating an artificial magnetic field for cavity photons. Two clouds of atoms are used for adiabatic flux insertion and strong interactions mediated by Rydberg atoms. (b) Structure of the photonic Landau levels labeled by orbital angular quantum number l and radial quantum number n. Here, $\Delta_{n,\alpha}$ is the frequency of the mode (n,α). The green box indicates the lowest Landau level (LLL). Initially, photons are pumped into the cavity mode with $n = l = 0$ (red arrow). Then, adiabatic flux insertion transfers orbital angular momentum (OAM) from a classical light beam to cavity photons, increasing the total angular momentum (blue arrow). (c) The density plot of the first three cavity modes in the LLL with angular momentum, from left to right, $l = 0$, $l = 3$, and $l = 6$.

fidelity of our protocol. In Sec. IV, we discuss the insertion of a single photon into the cavity and the strong photon-photon interactions to prepare the LN state. Finally, in Sec. V, we summarize our findings.

II. PHOTON CAVITY SETUP

The artificial magnetic field in the photonic cavity setup of Ref. [20] is created by using the similarity between the Lorentz force on a charged particle in a magnetic field and the Coriolis force. Consider a ring resonator, as indicated in Fig. 1(a), which confines the photon gas to a two-dimensional plane and leads to an effective mass. The mirror curvature modifies the mass and creates an additional harmonic potential in the two-dimensional plane. Using a nonplanar geometry leads to an image rotation of the transverse mode profile in a single roundtrip. This is equivalent to the action of an effective magnetic field pointing in the direction of propagation plus an antibinding centrifugal potential [21]. For sufficiently strong rotation the antibinding potential can compensate the harmonic confinement and Landau levels emerge. Such a configuration is, however, unstable and sensitive to astigmatism, which drives transitions between angular momentum states with difference $\Delta\ell = \pm 2$. Increasing the effective rotation even further eventually leads to another configuration with large degeneracy that is stable, containing angular momentum states which differ by multiples of $3\hbar$—the *photonic Landau levels*. The corresponding spectrum is illustrated in Fig. 1(b). Now, within each photonic Landau level with frequency $\Delta_{n,\alpha}$ labeled by the radial quantum number n and a fixed value of $\alpha = 0, 1, 2$, the photon angular momentum $\ell\hbar = (3m + \alpha)\hbar$ increases in multiples of $3\hbar$. The corresponding Hamiltonian is

$$H_0 = \hbar \sum_{\alpha=0}^{2} \sum_{n=0}^{\infty} \Delta_{n,\alpha} \sum_{m=0}^{\infty} a^{\dagger}_{n,3m+\alpha} a_{n,3m+\alpha}. \tag{1}$$

Here, $a^{\dagger}_{n,l}$ and $a_{n,l}$ are the creation and annihilation operators of a cavity photon in spatial mode $f_{n,l}(r,\phi)$, described by the Laguerre-Gauss (LG) eigenmodes,

$$f_{n,l}(r,\phi) = \sqrt{\frac{2^{|l|+1} n!}{\pi (|l|+n)! w_0^2}}\, x^{|l|} e^{il\phi} e^{-x^2} L_n^{|l|}(2x^2). \tag{2}$$

Here we defined $x = r/w_0$, with w_0 being the cavity waist and $L_n^{|l|}(x)$ are the LG polynomials. We use the term lowest Landau level (LLL) referring to the degenerate modes with radial quantum number $n = 0$ and $\alpha = 0$ (i.e., $l = 0, 3, 6, \ldots$).

It is convenient to express the cavity-field operator $\mathscr{E} = \sum_{\alpha=0}^{2} \sum_n \mathscr{E}_{n,\alpha}$ according to the photonic Landau-level structure as

$$\mathscr{E}_{n,\alpha}(r,\phi) = \sum_{m=0}^{\infty} f_{n,3m+\alpha}(r,\phi) a_{n,3m+\alpha}. \tag{3}$$

We note that all modes except $l = 0$ have a vanishing amplitude at the origin $r = 0$ and thus do not couple to atoms in the center of the transverse mode profile. More details of the experimental setup and mode functions can be found in Refs. [20,21] and in Appendix A.

The frequencies of all cavity modes with $n \neq 0$ [see Fig. 1(b)] are assumed to be far away from all atomic resonances, and coupling to them is thus disregarded in what follows and we use the shorthand notation $a_{0,3m} \to a_{3m}$, etc.

III. ADIABATIC FLUX INSERTION WITHOUT INTERACTION

A. Principle

The idea of adiabatically inserting flux quanta was introduced by Laughlin and provides an explanation of the quantized Hall current [29]. In the case of the photonic Landau levels, we insert *photonic flux quanta* in multiples of $3\hbar$. This leads to a controlled *parallel* transfer of photons from modes a_{3m} to a_{3m+3} within the LLL. To avoid any direct coupling between these two modes, which would lead to errors, we split the process into two successive steps:

$$\text{(i)}\ \ a_{3m} \to a_{3m+1}, \quad \text{(ii)}\ \ a_{3m+1} \to a_{3m+3}. \tag{4}$$

Light beams with OAM have already been successfully used to transfer angular momentum to an atomic medium [30]. Here we transfer OAM from an external light beam to the cavity photons utilizing an atomic medium as a mediator. We consider atoms with four relevant states, as depicted in Fig. 2(a). The atomic states are coupled via the cavity fields and external coherent driving fields carrying OAM l and with Rabi frequencies $\bar{\Omega}_l$. In order to be able to switch on and off the coupling of the cavity modes to the atomic medium, we assume that these transitions are sufficiently far away from single-photon resonance, but that all Raman transitions are in two-photon resonance. In this way, there is no interaction of the cavity field with the atomic medium in the absence of the classical driving fields.

In the first step (i), two classical laser fields, $\bar{\Omega}_1(r,\phi,t)$ and $\bar{\Omega}_0(r,t)$, which carry a net OAM of $1\hbar$ are applied to the atomic system. As a result, a set of dark states is created in the subspace of states with $n = 0$ which are mixtures

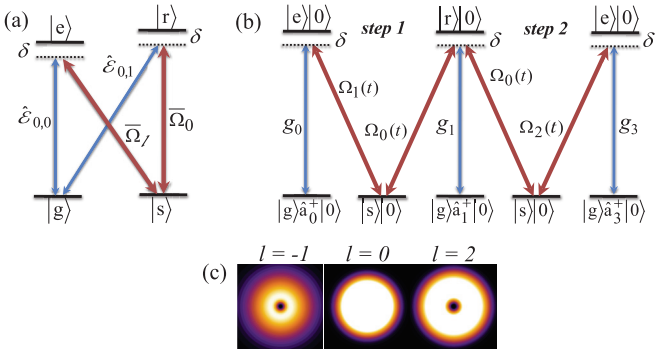

FIG. 2. (a) The atomic level structure consists of two metastable levels $|g\rangle$, $|s\rangle$ and two excited levels $|e\rangle$ and $|r\rangle$. (b) System initially prepared in state with $l = 0$. In the first stage of the protocol, the cavity modes $l = 0$ and $l = 1$ drive the transitions $|g\rangle \leftrightarrow |e\rangle$, $|g\rangle \leftrightarrow |r\rangle$ with coupling strength g_0 and g_1, while the laser fields $\Omega_1(t)$, $\Omega_0(t)$ couple the transitions $|e\rangle \leftrightarrow |s\rangle$, $|s\rangle \leftrightarrow |r\rangle$. We assume that the laser field Ω_1 has an OAM $-1\hbar$. As a consequence of this, the initial photon in the $l = 0$ mode is transferred to the $l = 1$ mode using the STIRAP technique. In the second step, the photon in the $l = 1$ mode is transferred to the $l = 3$ mode which belongs to the LLL manifold. This transition is performed by using the same atomic level structure, but with new Rabi frequency Ω_2 which carriers OAM $2\hbar$. (c) Density plots of the classical driving fields. We assume that the Ω_0 Rabi frequency has a Gaussian shape with $l = 0$. The other two classical laser fields carry OAM and thus have vanishing intensity at the center.

essentially between the cavity-field operators a_{3m} and a_{3m+1}; see Fig. 2(b). By using time-varying laser fields in a STIRAP counterintuitive pulse order, photons are absorbed from modes a_{3m} and successively created in modes a_{3m+1}. In this step, an OAM of $1\hbar$ is transferred to each cavity photon in parallel.

In the second step (ii), classical light fields $\bar{\Omega}_0(r, t)$ and $\bar{\Omega}_2(r, \phi, t)$ with net OAM of $2\hbar$ are used. This leads to the formation of a new set of dark states now involving photonic modes a_{3m+1} and a_{3m+3}; see Fig. 2(b). In this step, adiabatic following of the dark state transfers OAM of $2\hbar$ to each cavity photon. By successively repeating the processes, one can increase the angular momentum of all occupied cavity modes in the LLL in parallel by multiples of $3\hbar$.

B. Atom-field interaction

Consider a dense ensemble of atoms with a four-level atomic structure as shown in Fig. 2(a). Besides a ground state $|g\rangle$ and a metastable state $|s\rangle$, we consider two excited states $|e\rangle$, $|r\rangle$ with finite lifetime. The atoms interact with the cavity field as well as with an external classical light beam with OAM. Here the transitions $|g\rangle \leftrightarrow |e\rangle$ and $|g\rangle \leftrightarrow |r\rangle$ are coupled to the cavity fields $\mathscr{E}_{0,0}$ and $\mathscr{E}_{0,1}$, while the atomic transitions $|s\rangle \leftrightarrow |e\rangle$ and $|s\rangle \leftrightarrow |r\rangle$ are driven by classical light fields with time-dependent Rabi frequencies $\bar{\Omega}_l(r, \phi, t)$ and $\bar{\Omega}_0(r, t) = \Omega_0(t)$. We assume an almost constant atomic density $n(r)$ in the central region of the light-matter interaction. As mentioned above, all transitions are assumed to be away from single-photon resonance with detuning δ but in respective two-photon resonance. In this case, turning off the classical light fields amounts to switching off the interaction of the cavity modes with the atoms altogether. The atom-light coupling Hamiltonian is given by

$$H_\phi = \hbar\delta \int d^2r(\sigma_{ee} + \sigma_{rr}) - \hbar \int d^2r \left[\sum_{m=0}^{\infty} g_{3m} f_{0,3m}(r, \phi) a_{3m}\sigma_{eg} + \bar{\Omega}_l \sigma_{es} + \bar{\Omega}_0 \sigma_{sr} + \sum_{m=0}^{\infty} g_{3m+1} f_{0,3m+1}(r, \phi) a_{3m+1}\sigma_{rg} + \text{H.c.} \right]. \quad (5)$$

The coupling strength g_l is given by the atomic transition dipole matrix elements d_{eg} and d_{rg} of the $\mathscr{E}_{0,0}$ and $\mathscr{E}_{0,1}$ transitions, respectively, and overlap integrals with the mode functions

$$g_{3m} \sim d_{eg} \int_0^{2\pi} d\phi \int_0^{\infty} dr \; r f_{n,3m}(r, \phi)\, n(r),$$
$$g_{3m+1} \sim d_{rg} \int_0^{2\pi} d\phi \int_0^{\infty} dr \; r f_{n,3m+1}(r, \phi)\, n(r). \quad (6)$$

In Eq. (5), we have introduced the standard continuous atomic flip operators $\sigma_{\mu,\nu}(\vec{r}, t) = \frac{1}{\Delta V} \sum_{j\in\Delta V} |\mu_j\rangle\langle\nu_j|$ defined on a small volume ΔV centered around position $\vec{r}$ containing $\Delta N \gg 1$ atoms, which fulfill the commutation relations $[\sigma_{\alpha,\beta}(\vec{r}), \sigma_{\mu,\nu}(\vec{r}')] = \delta(\vec{r} - \vec{r}')[\delta_{\beta,\mu}\sigma_{\alpha,\nu}(\vec{r}) - \delta_{\alpha,\nu}\sigma_{\mu,\beta}(\vec{r})]$.

Initially, all atoms are in the ground state. We assume weak cavity fields and discuss the linear response regime. Then, we can approximately set $\sigma_{gg} \approx 1$ [31]. Thus, the only relevant operators for our discussion are the coherences of excited and ground states, $P = \sigma_{ge}$ and $R = \sigma_{gr}$, and the coherence between the ground state and metastable state, $S = \sigma_{gs}$. Within this approximation, the operators $A = P, R, S$ fulfill the commutation relation $[A(\vec{r}), A^\dagger(\vec{r}')] = \delta(\vec{r} - \vec{r}')$. It is convenient to decompose them also into the LG basis (2),

$$A(r, \phi) = \sum_{n,l=0}^{\infty} A_{n,l}\, f_{n,l}(r, \phi). \quad (7)$$

C. First step

In the first step of the flux insertion scheme, we assume that the laser field $\bar{\Omega}_l(r, \phi, t)$ in Eq. (5) has $l = 1$, i.e., carries an OAM of $-1\hbar$ such that

$$\bar{\Omega}_1(r, \phi, t) = \Omega_1(t)\, \kappa_1(x)\, e^{-i\phi}. \quad (8)$$

Now, using the decomposition of the atomic modes (7) and the photonic cavity modes (3), we can easily evaluate the Hamiltonian given by Eq. (5). Including the photonic Landau-level Hamiltonian (1), we derive the Heisenberg-Langevin equations in the linear response regime,

$$\frac{d}{dt} P_{n,3m} = -(i\delta + \gamma) P_{n,3m} + i\Omega_1 \sum_{n'=0}^{\infty} \chi_{3m}^{n,n'} S_{n',3m+1} + i g_{3m} a_{3m} \delta_{n,0},$$
$$\frac{d}{dt} S_{n,3m+1} = i\Omega_1^* \sum_{n'=0}^{\infty} \left(\chi_{3m}^{n',n}\right)^* P_{n',3m} + i\Omega_0 R_{n,3m+1},$$
$$\frac{d}{dt} R_{n,3m+1} = -(i\delta + \gamma) R_{n,3m+1} + i\Omega_0^* S_{n,3m+1} + i g_{3m+1} a_{3m+1} \delta_{n,0},$$

$$\frac{d}{dt}a_{3m} = ig_{3m}P_{0,3m},$$
$$\frac{d}{dt}a_{3m+1} = ig_{3m+1}R_{0,3m+1}, \tag{9}$$

with coupling coefficients determined by

$$\chi_{3m}^{n,n'} = \int_0^{2\pi} d\phi \int_0^{\infty} dr\, r\kappa_1(r)e^{-i\phi} f_{n,3m}^{*}(r,\phi)\, f_{n',3m+1}(r,\phi). \tag{10}$$

Here, γ is the spontaneous decay rate from the excited states $|e\rangle$ and $|r\rangle$, which we assume for simplicity to be equal. Note that in the linear response regime, the population of the excited states is negligible, which allows us to neglect Langevin noise terms here. We also disregard the cavity decay in our description for now, but include it later in Sec. IV.

One recognizes from Eqs. (9) that there is in general a coupling between modes with different radial index n, which is a problem. For that reason, we now choose the spatial profile $\kappa_1(x)$ in such a way that couplings from the $n = 0$ spin modes $S_{0,3m+1}$ to higher modes with $n' > 0$ are highly suppressed, i.e., such that $\chi_{3m}^{n',0} \sim \delta_{n',0}$. This can be achieved for $\kappa_1(x) = 1/x$ with $\chi_{3m}^{0,0} = \sqrt{\frac{2}{3m+1}}$; see Eq. (10). Then, one can directly construct a dark state for an OAM transfer of $\Delta\ell = 1$,

$$\Psi_m^{(1)} = \frac{1}{N_m}\left\{ g_{3m+1}\sqrt{\frac{2}{3m+1}}\Omega_1\, a_{3m} + g_{3m}\Omega_0 a_{3m+1} - g_{3m}g_{3m+1}S_{0,3m+1}\right\}, \tag{11}$$

which is a superposition of cavity-field operators a_{3m}, a_{3m+1} and the corresponding collective ground-state coherences. It is straightforward to show that the dark state is a constant of motion in the adiabatic limit, i.e., $\partial_t \Psi_m^{(1)} = 0$. Here, $N_m(t)$ is a normalization factor. We note that there is no choice of spatial profile $\kappa_1(x)$ that also simultaneously and perfectly suppresses the couplings $\chi_{3m}^{0,n'}$ of the $n = 0$ optical polarization modes $P_{0,3m}$ to modes with $n' > 0$. However, this is not a necessary condition to construct a dark state. Indeed, the couplings $\chi_{3m}^{0,n'}$ between the LLL ($n = 0$) with higher Landau level ($n' \geqslant 1$) are all of the order of unity for $\kappa_1(x) \sim 1/x$, i.e., $\chi_{3m}^{0,n'} = \mathcal{O}(1)$.

The ideal spatial profile $\kappa_1 \sim 1/x$ cannot be realized experimentally, however, since $\bar{\Omega}_1$ carries a nonvanishing OAM and thus must vanish for $r \to 0$. Instead, we choose

$$\kappa_1(x) = \frac{x^2}{a^3 + x^3}, \tag{12}$$

where $a = r_0/w_0$ and $r_0 \ll w_0$ is some cutoff length. In the limiting case $a \to 0$, this approaches the ideal profile. For $a \ll 1$, the couplings $|\chi_{3m}^{n',0}| \sim a^2 \ll \chi_{3m}^{0,0}$ are strongly suppressed (see Appendix A) and we approximately obtain the dark state given by Eq. (11). The small residual couplings to collective atomic modes with higher radial index $n' > 0$ will lead to some losses, which will be discussed in Sec. III E.

Now a fully adiabatic transfer of excitations can be performed using a STIRAP protocol. As long as $\Omega_1 \gg \{\Omega_0(t_i)\sqrt{\frac{3m+1}{2}}\frac{g_{3m}}{g_{3m+1}}, g_{3m}\}$, the dark states coincide with the initial state, $\Psi_m^{(1)} \simeq a_{3m}$. Adiabatic following transfers the dark states into $\Psi_m^{(1)} \simeq a_{3m+1}$ if $\Omega_0 \gg \{\Omega_1\sqrt{\frac{2}{3m+1}}\frac{g_{3m+1}}{g_{3m}}, g_{3m+1}\}$, which concludes the first step of the protocol at time t_1, and the population from all modes a_{3m} of the LLL is transferred in parallel to modes a_{3m+1} which belong to an excited Landau-level manifold with $\alpha = 1$.

In order to return the population back to the LLL manifold, we repeat the same procedure as above using the same atomic structure but with new Rabi frequency $\bar{\Omega}_2$, as we explain in the following.

D. Second step

The goal of the second step is to increase the angular momentum of all photons by $2\hbar$. In order to perform this, we assume that the transition $|e\rangle \leftrightarrow |s\rangle$ is driven with Rabi frequency

$$\bar{\Omega}_2(r,\phi,t) = \Omega_2(t)\kappa_2(x)e^{2i\phi}, \tag{13}$$

which carriers OAM $2\hbar$. Consequently, we obtain a similar Heisenberg-Langevin equation to Eq. (9),

$$\begin{aligned}
\frac{d}{dt}P_{n,3m+3} &= -(i\delta+\gamma)P_{n,3m+3} + i\Omega_2\sum_{n'=0}^{\infty}\tilde{\chi}_{3m+3}^{n,n'}S_{n',3m+1} \\
&\quad + ig_{3m+3}a_{3m+3}\delta_{n,0}, \\
\frac{d}{dt}S_{n,3m+1} &= i\Omega_2^{*}\sum_{n'=0}^{\infty}\left(\tilde{\chi}_{3m+3}^{n',n}\right)^{*}P_{n',3m+3} + i\Omega_0 R_{n,3m+1}, \\
\frac{d}{dt}R_{n,3m+1} &= -(i\delta+\gamma)R_{n,3m+1} + i\Omega_0^{*}S_{n,3m+1} \\
&\quad + ig_{3m+1}a_{3m+1}\delta_{n,0}+, \\
\frac{d}{dt}a_{3m+3} &= ig_{3m+3}P_{0,3m+3}, \\
\frac{d}{dt}a_{3m+1} &= ig_{3m+1}R_{0,3m+1},
\end{aligned} \tag{14}$$

with new coupling coefficients,

$$\tilde{\chi}_{3m}^{n,n'} = \int_0^{2\pi} d\phi \int_0^{\infty} dr\, r\kappa_2(x)e^{2i\phi}\, f_{n,3m}^{*}(r,\phi)\, f_{n',3m-2}(r,\phi). \tag{15}$$

We now choose the spatial profile of $\kappa_2(x)$ in such a way that couplings from the $n = 0$ spin modes $S_{0,3m+1}$ to higher modes with $n' > 0$ are highly suppressed, i.e., that $\tilde{\chi}_{3m+3}^{n',0} \sim \delta_{n',0}$. This can be achieved for $\kappa_2(x) = x^2$ with $\tilde{\chi}_{3m+3}^{0,0} = \frac{1}{2}\sqrt{\frac{(3m+3)!}{(3m+1)!}}$. Note that with this experimentally feasible choice of the spatial profile, all couplings of spin coherences $S_{0,3m+1}$ to higher states with $n' > 0$ are exactly canceled such that there are no undesired residual couplings.

Similarly, we can directly construct an infinite set of dark states,

$$\Psi_m^{(2)} = \frac{1}{\tilde{N}_m}\left\{ g_{3m+1}\frac{\Omega_2}{2}\sqrt{\frac{(3m+3)!}{(3m+1)!}}a_{3m+3} + g_{3m+3}\Omega_0 a_{3m+1} - g_{3m+3}g_{3m+1}S_{0,3m+1}\right\}, \tag{16}$$

which are a constant of motion in the adiabatic limit, i.e., $\partial_t \Psi_m^{(2)} = 0$.

Starting at time t_1, which is now the initial time for the second step, the dark state (16) coincides with $\Psi_m^{(2)} \simeq a_{3m+1}$ as long as $\Omega_0 \gg \{\Omega_2 \frac{1}{2}\sqrt{\frac{(3m+3)!}{(3m+1)!}}\frac{g_{3m+1}}{g_{3m+3}},\ g_{3m+1}\}$. Adiabatically increasing $\Omega_2(t)$ drives the system into $\Psi_m^{(2)}(t_f) \simeq a_{3m+3}$ if at $t = t_f$: $\Omega_2 \gg \{2\sqrt{\frac{(3m+1)!}{(3m+3)!}}\Omega_0\frac{g_{3m+3}}{g_{3m+1}},\ g_{3m+3}\}$, which concludes the second step. In total, the flux insertion protocol transfers OAM in multiples of $3\hbar$ to all cavity modes of the LLL in parallel.

E. Imperfections

In the following, we discuss the corrections that limit the fidelity of the adiabatic flux insertion. There are two main sources of imperfections. The first one is the small residual off-resonant couplings $\chi_{3m}^{n',0}$ to cavity modes with $n' > 0$. The second one is the violation of adiabaticity, in particular in the center of the atomic cloud, due to the vanishing amplitude of the classical light fields $\bar{\Omega}_l$ with $l \neq 0$.

1. Residual couplings to higher collective atomic levels with n > 0

In the first step of the scheme, we neglected residual coupling $S_{0,3m+1} \leftrightarrow P_{n,3m}$ with $n \neq 0$. This would be correct for the ideal spatial profile, $\kappa_1(x) \sim 1/x$. For the realistic profile, given by Eq. (12), there is a residual coupling, however, leading to excitations of state $|e\rangle$, which spoils the adiabatic transition. We find that in the lowest order of a, the residual coupling strengths scale as

$$\chi_0^{n',0} \simeq -\frac{8\pi}{3}\sqrt{\frac{2}{3}}a^2, \tag{17}$$

for $m = 0$. For higher m, the $\chi_{3m}^{n',0}$ become even smaller. Thus the condition $a \ll 1$ ensures the suppression of the undesired couplings to excited LL.

As an example, let us consider the following time-dependent Rabi frequencies:

$$\bar{\Omega}_1(r,\tau) = \kappa_1(x)\frac{\Omega}{\sqrt{1+e^{\tau}}}, \quad \bar{\Omega}_0(\tau) = \frac{\Omega}{\sqrt{1+e^{-\tau}}}, \tag{18}$$

which can be used to drive the first stage of the scheme. Here, Ω is the peak Rabi frequency and $\tau = t/T$, where T is the characteristic pulse length. Assume that the pulses are applied in counterintuitive order in the time interval $[-\tau_1, \tau_1]$ such that $\Omega_1(-\tau_1) \gg \Omega_0(-\tau_1)$ and, respectively, $\Omega_1(\tau_1) \ll \Omega_0(\tau_1)$. For the second stage, we use

$$\bar{\Omega}_2(r,\tau) = \kappa_2(x)\frac{\Omega}{\sqrt{1+e^{2\tau_1-\tau}}}, \quad \bar{\Omega}_0(\tau) = \frac{\Omega}{\sqrt{1+e^{\tau-2\tau_1}}}, \tag{19}$$

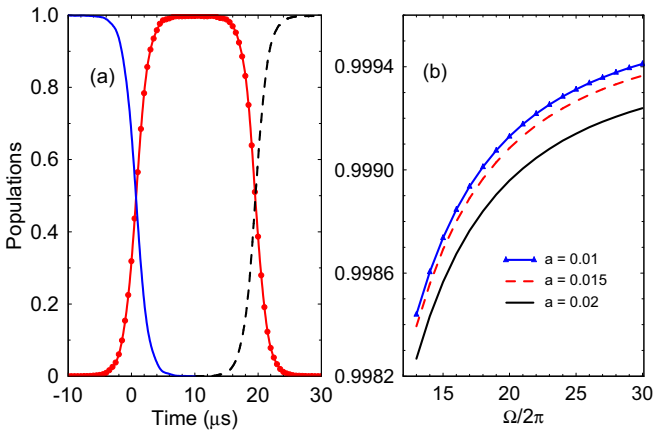

FIG. 3. (a) The expectation values of $a_{0,l}$ ($l = 0, 1, 3$) vs time. The exact result for $a_{0,0}$ (blue line) and $a_{0,1}$ (dotted red line) according the coupled system (9) including the residual couplings for $a = 10^{-2}$. The dashed black line shows the time evolution of $a_{0,3}$ according to the coupled system (14). We choose time-dependent Rabi frequencies (18) and (19) with $\Omega = (2\pi)12.4$ MHz and cavity couplings $g = (2\pi)0.45$ MHz. The other parameters are set to $\gamma = 0$, $\delta = (2\pi)0.13$ MHz and $T = 1$ μs. (b) The expectation value of $a_{0,1}$ at time t_1 against Ω for different cutoff length.

which guarantees that $\Omega_2(\tau_f) \gg \Omega_0(\tau_f)$. In Fig. 3(a), we plot the exact time evolution of the probabilities for adiabatic transition. As can be seen, including small cutoff length a, the respective residual couplings do not affect the adiabatic flux insertion. Increasing the peak Rabi frequency Ω further suppresses the nonadiabatic transition; see Fig. 3(b).

2. Nonadiabatic losses

The OAM transferred to the cavity photons in the flux insertion is taken from the classical laser fields $\bar{\Omega}_l$ with $l \neq 0$. These fields necessarily have a vanishing intensity at the origin $r = 0$ and thus adiabaticity is violated in the center of the atom cloud. Instead of following adiabatically the dark state, atoms close to the center will be excited into the intermediate states due to absorbtion of cavity photons. As a consequence of that, there is a leak of population from the dark-state subspace during both steps of the protocol. In the following, we assume a worst-case scenario where the optical fields are on resonance. The finite detuning δ further suppresses these errors.

The total amount of nonadiabatic losses can be obtained by calculating the number of atoms not returning to the initial state after a full cycle of the protocol. The probability of an atom at distance r from the center to remain in the adiabatic state during the first stage of the protocol can be estimated as (see Appendix B)

$$e_1(\vec{r}) = \exp\left\{-\frac{2\gamma}{g^2}\int_{t_i}^{t_1} dt\left[\dot{\varphi}_1^2\sin^2(\theta_1) + \dot{\theta}_1^2\cos^2(\theta_1)\right]\right\}, \tag{20}$$

where we have assumed, for simplicity, that $g_{3m} = g_{3m+1} = g$. Here, $\varphi_1(r,t) = \tan^{-1}[\bar{\Omega}_0(t)/\bar{\Omega}_1(r,t)]$ and $\theta_1(r,t) = \tan^{-1}[\sqrt{\bar{\Omega}_1^2(r,t) + \bar{\Omega}_0^2(r,t)}/g]$ are the time-dependent mixing angles. For the Rabi frequencies (18), one can evaluate the probability (20); see Appendix B.

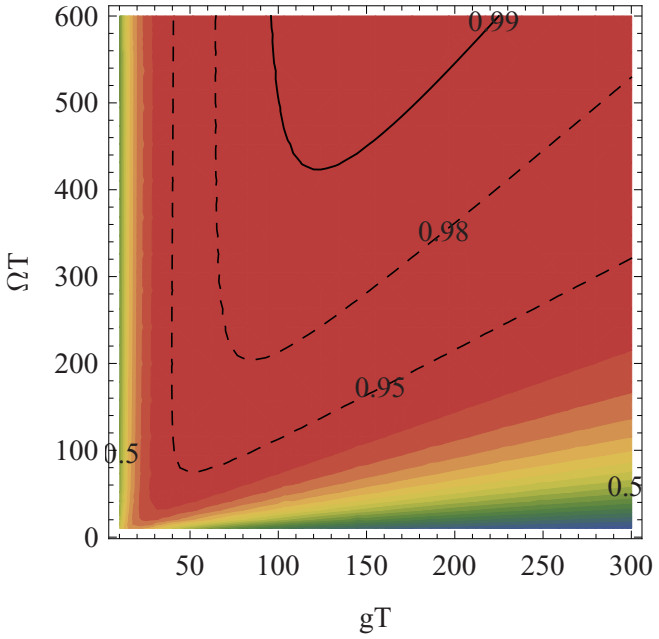

FIG. 4. Fidelity of the flux insertion scheme vs the peak Rabi frequency ΩT and cavity coupling gT according to Eq. (24). We assume Gaussian distribution of the atomic density. The parameters are $\gamma T = 100$, $a = 0.005$, and $\xi = 0.25 w_0$.

Similarly, the probability for an atom at position r to remain in the dark-state subspace during the second stage is given by

$$e_2(\vec{r}) = \exp\left\{ -\frac{2\gamma}{g^2} \int_{t_1}^{t_f} \left[\dot{\varphi_2}^2 \sin^2(\theta_2) + \dot{\theta_2}^2 \cos^2(\theta_2)\right] \right\}, \tag{21}$$

where now $\varphi_2(r,t) = \tan^{-1}[\bar{\Omega}_2(r,t)/\bar{\Omega}_0(t)]$ and $\theta_2(r,t) = \tan^{-1}[\sqrt{\bar{\Omega}_2^2(r,t) + \bar{\Omega}_0^2(t)}/g]$.

The total probability for all atoms to stay in the dark state after a full cycle of operation thus reads

$$p = \frac{\int d^2r\ n(\vec{r})\, e_1(\vec{r})\, e_2(\vec{r})}{\int d^2r\ n(\vec{r})}. \tag{22}$$

Furthermore, one has to take into account that the system is prepared at the beginning of a full cycle in a state with a single photon in mode $f_{0,0}$ and all atoms in the ground state $|g\rangle$. This state does not have a perfect overlap with the dark state, but the latter reads

$$p_{\text{in}} = \frac{1}{N} \int d^2r\, \frac{\Omega_1^2 \kappa_1^2(r)}{g^2 + \Omega_1^2 \kappa_1^2(r)}\, n(\vec{r}), \tag{23}$$

where we have used that initially $\bar{\Omega}_0(t_i) = 0$.

This gives, for the fidelity of the flux insertion,

$$F = p p_{\text{in}}. \tag{24}$$

In Fig. 4, we have plotted the fidelity as a function of the peak Rabi frequency ΩT and the cavity coupling gT assuming Gaussian distribution of the density of atoms, $n(r) = n_0 e^{-r^2/\xi^2}$ with $n_0 = N/\pi\xi^2$. As can be expected, increasing gT compared to γT leads to smaller absorption length, which improves the fidelity. However, for sufficiently high gT compared to ΩT, the respective overlap between the initial state and the dark state becomes smaller, which limits the fidelity.

IV. LAUGHLIN STATE PREPARATION

Now, we discuss the preparation of Laughlin-type states in a setup of cavity Rydberg polaritons. Following Refs. [23,24], a Laughlin state can be grown by the successive repetition of adiabatic flux insertion (see Sec. III) and a single-photon coherent pump, discussed below.

A. Rydberg cavity polaritons and Laughlin state

To realize a fractional quantum Hall system requires, besides the artificial magnetic field discussed in Sec. II and Ref. [20], strong interactions between the photonic cavity modes in the lowest photonic Landau level,

$$H_{\text{int}} = \sum_{l_1,l_2} \sum_{l_3,l_4} V_{l_3,l_4}^{l_1,l_2}\, a_{l_1}^\dagger a_{l_2}^\dagger a_{l_3} a_{l_4}, \tag{25}$$

where $l_i = 3m$ and $m = 0, 1, \ldots$. This Hamiltonian can be realized by coupling the cavity field $\mathscr{E}_{0,0}$ to a high-lying Rydberg state in an EIT configuration [8,27,28]. In recent cavity experiments, the strong nonlinearity on the single-photon level was demonstrated [32,33]. The Rydberg cavity polaritons have an effective interaction potential, $V(r) = C_6/(r^6 + a_B^6)$. Here, C_6 is the effective interaction strength and a_B is the Rydberg blockade radius. Although the opposite regime is very interesting in its own right [34], we assume in the following the case where the magnetic length $l_B = w_0/2$ is much larger than a_B. In this limit, the dominant interaction contribution comes from the zero's Haldane pseudopotential [34],

$$V_0 \simeq \frac{3C_6}{8 l_B^2 a_B^4}, \tag{26}$$

which determines all interaction coefficients [35],

$$\begin{aligned} V_{l_3,l_4}^{l_1,l_2} &= \langle l_1, l_2 | V | l_3, l_4 \rangle \\ &\simeq \frac{V_0}{2} (l_1 + l_2)! \sqrt{\frac{2^{-2(l_1+l_2)}}{l_1! l_2! l_3! l_4!}}\, \delta_{l_1+l_2, l_3+l_4}. \end{aligned} \tag{27}$$

We assume for the interaction coefficients $V_{l_3,l_4}^{l_1,l_2} \ll |\Delta_{0,1} - \Delta_{0,0}|$, i.e., they are small compared to the energy gap between the Landau levels to avoid mixing of states in a different Landau level.

The combination of the photonic Landau level given by Eq. (1) and the strong photon nonlinearity given by Eq. (25) lead to a set of degenerate low-energy states with total angular momentum L depending on the photon number N [20,22,36]. For a given photon number N, the zero-energy state with lowest total angular momentum,

$$\langle z_1, \ldots, z_N | \text{LN}, N \rangle = \prod_{i<j} \left(z_i^3 - z_j^3\right)^2, \tag{28}$$

is a unique ground state of the system [36], which resembles a Laughlin (LN)-type state. Here we have dropped the ubiquitous Gaussian factor and the normalization constant [20,36]. The two-dimensional coordinate is $z_j = x_j - i y_j$. The total angular momentum of the state (28) with N photons is $L|\text{LN}, N\rangle = 3N(N-1)|\text{LN}, N\rangle$. In addition, we consider here the mth

quasihole states with N photons,

$$\langle z_1, \ldots, z_N | \mathrm{qh}_m \rangle = \prod_k z_k^{3m} \prod_{i<j} \left(z_i^3 - z_j^3\right)^2, \qquad (29)$$

having total angular momentum $L|\mathrm{qh}_m, N\rangle = \frac{3}{2}mN(N+1)|\mathrm{qh}_m, N\rangle$. It is straightforward to show that the Laughlin-type state with $N+1$ photons has the same total angular momentum as the two-quasihole state with N photons.

B. Full protocol

Single-photon pump. We consider a coherent pump which injects a single photon into the mode a_0. This implies that there is no transfer of angular momentum into the system. We assume that an external laser field is applied with mode profile matching the $l = 0$ angular momentum state,

$$H_{\Omega_p} = \Omega_p (a_0^\dagger e^{-i\omega t} + a_0 e^{i\omega t}). \qquad (30)$$

Here, Ω_p is the driving pump Rabi frequency into the cavity and ω is the oscillation frequency which we assume to be in resonance with respect to the energy of the LLL, i.e., $\omega = \Delta_{0,0}$. Without the interaction given by Eq. (25), the Hamiltonian (30) creates a coherent amplitude of the photonic mode which contains a superposition of many photons. However, strong photon blockade ensures the insertion of a single photon requiring $\Omega_p \ll V_0, \Delta_{\mathrm{LN}}$, where $\Delta_{\mathrm{LN}} \simeq 0.2V_0$ is the many-body gap of the system. Note that the Laughlin gap only slightly depends on the photon number N. Starting from a two-quasihole state $|2\mathrm{qh}, N\rangle$, we use a π pulse of time $\tau_p = \pi/2\Omega^{(N)}$, where

$$\Omega^{(N)} = \Omega_p \langle \mathrm{LN}, N+1 | a_0^\dagger | 2\mathrm{qh}, N \rangle \qquad (31)$$

is the coupling between the quasihole and Laughlin state [23,24], to insert a single photon.

Adiabatic flux insertion. In Sec. III, we discussed the noninteracting case for inserting flux quanta by transferring all photons to the first Landau level and then back to the LLL. Now, in the interacting case, we require adiabaticity $\Delta_{\mathrm{LN}}\tau_{\mathrm{f}} \gg 1$, where the many-body gap Δ_{LN} should not vanish during flux insertion. To this end, we couple the photonic cavity field $\mathscr{E}_{0,1}$ in the first Landau level using an EIT scheme to a Rydberg state as well. This ensures maintenance of a finite many-body gap Δ_{LN}. For simplicity, we assume the same interaction potential $V(r)$ as before. Now, in Eq. (25), we sum over all photonic modes in the lowest and first Landau level.

Protocol. The growing scheme is depicted in Fig. 5. It starts by preparing the cavity with no photon. Then, in the first step, a single photon in mode a_0 is pumped into the cavity $|0\rangle \to a_0^\dagger|0\rangle$ by using the nonlinear interaction (25). This state obviously has total angular momentum $L = 0$. Next, we repeat the flux insertion scheme in Sec. III two times, which realizes the transition $a_0^\dagger|0\rangle \to a_6^\dagger|0\rangle$ with $L = 6$. The latter state is a two-quasihole state with one photon. Now a second photon is pumped into the cavity. The finite overlap $\Omega^{(1)}/\Omega_p = \sqrt{10/11}$ with the Laughlin state ensures that we pump into the ground state of the system. This step creates a Laughlin state with $N = 2$ photons. By repeating these two steps, we grow a Laughlin-type state (28) with N photons.

To numerically simulate the full growing protocol is rather involved, since taking into account all different atomic excitations leads to fast growing of the relevant Hilbert space even for few excitations. Therefore, we simplify the protocol, reducing it to the essential components, namely, the adiabatic increase of angular momentum of the cavity modes by flux insertion and subsequent photon insertion. The simplified flux insertion method used for the simulation relies solely on the photonic cavity modes and is therefore amenable to numerical simulations by exact diagonalization. Specifically, we consider a direct coupling between the lowest and first Landau level and change the energies of the Landau levels in time. This resembles a rapid adiabatic passage sweep. In Appendix C, we explain the method in detail. In Fig. 6, we show a numerical simulation of the full protocol for the preparation of Laughlin states up to three photons. After three steps of the protocol, we obtain a LN state with three photons with probability $|\langle\psi|\mathrm{LN}, 3\rangle|^2 \approx 0.97$.

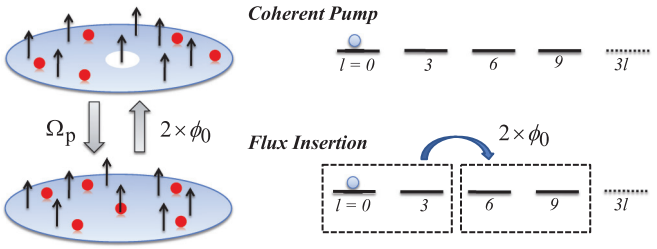

FIG. 5. The growing scheme which is used for the preparation of the Laughlin-type states consists of two steps. (i) Coherent pump of a single photon in the ground state of the cavity by using the nonlinear photon-photon interaction. (ii) Increase of angular momentum per particle by 6 (flux insertion). Repeating the two steps lead to growing of the photonic Laughlin-type state.

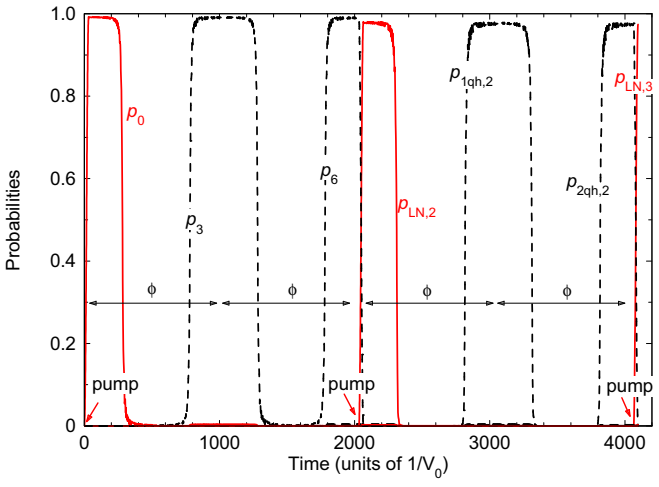

FIG. 6. Numerical simulation of growing scheme for the creation of Laughlin states with $N = 2$ and $N = 3$ photons. The system is prepared initially in a state with no photon. The red arrow indicates the time at which the coherent pump is applied. The angular momentum per photon is increased by repeating the flux insertion twice. The probabilities are $p_m = |\langle\psi|a_m^\dagger|0\rangle|^2$, and, respectively, $p_{\mathrm{LN},N}$ and $p_{\mathrm{qh}_m,N}$ are the probabilities for the Laughlin state and mth-quasihole state. The adiabatic flux insertion method for numerical simulation is explained in Appendix C. The parameters are set to $\Delta_0/V_0 = 10$, $\Omega_p/V_0 = 1/20$, and $g_a/V_0 = g_b/V_0 = 1/5$.

Finally, let us comment on the fidelity of our scheme. On the one hand, in the flux insertion process (see Sec. III E), the imperfections come from nonadiabatic transitions, which requires $\Omega_l \tau_\mathrm{f} \gg 1$, $\Delta_\mathrm{LN} \tau_\mathrm{f} \gg 1$. On the other hand, in the coherent pump, the imperfections come from coupling to higher photon-number states which require $\Delta_\mathrm{LN} \tau_p \gg 1$. While both favor large timescales $\tau = 2\tau_\mathrm{f} + \tau_p$ for each step in the growing protocol, losses limit the timescale τ. We take into account the effect of cavity losses as well as the finite lifetime of the Rydberg state by an effective loss rate γ_eff. As shown in Refs. [23,24], the fidelity for the creation of an N-photon Laughlin state then scales as

$$\mathscr{F}_N \simeq \exp\left\{ -\frac{1}{2} N \left[\frac{1}{2} \gamma_\mathrm{eff} \tau (N+1) + \frac{\Lambda_N^2}{(\Delta_\mathrm{LN} \tau)^2} \right] \right\}, \quad (32)$$

where Λ_N depends on photon number N. Note that our protocol first creates a hole excitation in the center and then refills the hole. Repeating the steps of the protocol, photons are pumped continuously into the center of the system. Defects created by losses will be continuously pumped to the periphery of the system and we expect that a much higher fidelity can be achieved in the steady state in the center of the cavity.

V. DISCUSSION AND OUTLOOK

In summary, we discussed an adiabatic transfer protocol to insert flux quanta in a photonic twisted-cavity setup. The scheme relies on a robust STIRAP technique transferring OAM of an external classical laser beam to the photonic cavity modes. A dense atomic ensemble hereby acts as a mediator. We show that the transfer can be described by a set of dark states between cavity modes with different angular momentum. Furthermore, we discuss imperfections of the protocol and estimate the fidelity. In addition, we discuss the preparation of Laughlin-type states based on the growing protocol of Refs. [23,24]. To this end, we discuss a single-photon pump coupling the cavity field to a high-lying Rydberg state in an EIT configuration. We show that by successive repetition of flux insertion and coherent pump, a Laughlin-type state can be prepared with high fidelity. Since, as compared to alternative growing protocols [25], in our scheme photons and thus also loss-induced defects are continuously pumped from the center to the periphery of the system, we expect to create Laughlin-type states with much higher fidelity in the center of the cavity.

The nonlocal character of the interaction between Rydberg polaritons may lead to other interesting states such as the Moore-Read Pfaffian [37] in the regime of large magnetic fields, where the magnetic length becomes comparable to or smaller than the blockade radius [34]. Furthermore, the coherent control may allow one to investigate bilayer quantum Hall phases, exploring different photonic Landau levels.

ACKNOWLEDGMENTS

This work was supported by the DFG through the priority program GiRyd (Grant No. SPP 1929). P.A.I. acknowledges support by the ERyQSenS, Bulgarian Science Fund Grant No. DO02/3. J.S. acknowledges support from MURI Grant No. FA9550-16-1-0323. F.L. is financially supported by a fellowship through the Excellence Initiative MAINZ (Grant No. DFG/GSC 266). The authors thank D. Dzsotjan for helpful discussions.

APPENDIX A: COUPLING MATRIX ELEMENTS

1. Properties of Laguerre-Gauss polynomials

The Laguerre-Gauss (LG) polynomials form a complete set of functions with the following orthogonal condition:

$$\int_0^\infty e^{-x} x^k L_n^k(x) L_m^k(x) dx = \frac{(n+k)!}{n!} \delta_{n,m}. \quad (A1)$$

For $n = 0$, we have $L_0^l(x) = 1$. The LG polynomials also obey the recurrence relations $L_n^{l-1}(x) = L_n^l(x) - L_{n-1}^l(x)$ and $\sum_{p=0}^n L_p^l(x) = L_n^{l+1}(x)$.

The mode functions $f_{n,l}$ in Eq. (2) fulfill the orthogonality relation

$$\int_0^{2\pi} d\phi \int_0^\infty dr \; r f_{n,l}^*(r,\phi) f_{n',l'}(r,\phi) = \delta_{l,l'} \delta_{n,n'}. \quad (A2)$$

2. First step

The coupling matrix elements of the first step are

$$\chi_{3m}^{n',n} = C_{3m}^{n',n} \int_0^\infty e^{-2x^2} x^{6m+2} \kappa_1(x) L_n^{3m+1}(2x^2) L_{n'}^{3m}(2x^2) dx, \quad (A3)$$

with $C_{3m}^{n',n} = 2^{3m+2} \sqrt{\frac{2n!n'!}{(3m+1+n)!(3m+n')!}}$. Here the function $\kappa_1(x)$ describes the intensity shape of the Rabi frequency $\bar{\Omega}_1$. We choose

$$\kappa_1(x) = \frac{x^2}{a^3 + x^3}, \quad (A4)$$

where $a = r_0/w_0$ is the dimensionless cutoff.

$a \to 0$ limit. Considering first the LLL, i.e., $n = 0$ and, making the substitution $y = 2x^2$, we have

$$\chi_{3m}^{n',0} = \sqrt{\frac{2n'!}{(3m+1)!(3m+n')!}} \int_0^\infty e^{-y} y^{3m} L_{n'}^{3m}(y) dy. \quad (A5)$$

Using the orthogonality given by Eq. (A1), we find

$$\chi_{3m}^{n',0} = \sqrt{\frac{2}{3m+1}} \delta_{n',0}. \quad (A6)$$

The general result for the coupling coefficient in the limit $a \to 0$ is

$$\chi_{3m}^{n',n} = \begin{cases} \sqrt{\frac{2(3m+n')!n!}{n'!(3m+1+n)!}} & \text{for} \quad n \geqslant n', \\ 0 & \text{for} \quad n < n'. \end{cases}$$

While the couplings $\chi_{3m}^{0,n'}$ between the lowest and higher Landau levels $n' \geqslant 1$ are of the order of unity even for $a \to 0$, all couplings $\chi_{3m}^{n',0}$ vanish identically.

Lowest-order corrections in a. The lowest-order correction of $\chi_{3m}^{n',0}$ in a for $m = 0$ is

$$\chi_0^{n',0} \approx -\frac{8\pi}{3} \sqrt{\frac{2}{3}} a^2 + \mathcal{O}(a^3) \quad (A7)$$

and becomes even smaller for $m > 0$. Thus, as long as $a \ll 1$, coupling to higher Landau levels is negligible.

3. Second step

In the second step, we choose $\bar{\Omega}_2(r,\varphi,t) = \Omega_2(t)\, x^2\, e^{2i\varphi}$, such that the coupling strengths become

$$\tilde{\chi}_{3m}^{n',n} = \tilde{C}_{3m}^{n',n} \int_0^\infty e^{-2x^2} x^{6m+1} L_n^{3m-2}(2x^2) L_{n'}^{3m}(2x^2) dx, \tag{A8}$$

with $\tilde{C}_{3m}^{n',n} = 2^{3m+1}\sqrt{\frac{n!n'!}{(3m-2+n)!(3m+n')}}$. Setting $n = 0$ and making the substitution $y = 2x^2$, we get

$$\tilde{\chi}_{3m}^{n',0} = \frac{1}{2}\sqrt{\frac{n'!}{(3m-2)!(3m+n')!}} \int_0^\infty e^{-y} y^{3m} L_{n'}^{3m}(y) dy. \tag{A9}$$

Finally, using the orthogonality (A1), we obtain

$$\tilde{\chi}_{3m}^{n',0} = \frac{1}{2}\sqrt{\frac{3m!}{(3m-2)!}}\delta_{n',0}, \tag{A10}$$

which implies that the transition to states with $n' > 0$ is completely suppressed.

APPENDIX B: NONADIABATIC LOSSES

Consider the five-level system driven by two cavity fields g_{3m} and g_{3m+1} and, respectively, two classical laser beams Ω_1 and Ω_0, as depicted in Fig. 2. Including the spontaneous decay from the two excites states, the non-Hermitian interaction Hamiltonian becomes

$$H = \begin{bmatrix} -i\gamma & \Omega_1 & 0 & g & 0 \\ \Omega_1 & 0 & \Omega_0 & 0 & 0 \\ 0 & \Omega_0 & -i\gamma & 0 & g \\ g & 0 & 0 & 0 & 0 \\ 0 & 0 & g & 0 & 0 \end{bmatrix}, \tag{B1}$$

where, for simplicity, we assume equal cavity couplings $g_{3m} = g_{3m+1} = g$. The time-dependent Schrödinger equation reads $i\hbar\frac{d}{dt}\vec{B} = H\vec{B}$, where column vector $\vec{B} = [c_e, c_s, c_r, c_{a_1}, c_{a_2}]^{\mathrm{T}}$ comprises the diabatic probability amplitudes of the five states. For $\gamma = 0$, the eigenspectrum of H consists of one zero-energy dark state,

$$|d\rangle = \cos(\varphi)\sin(\theta)|a_0\rangle + \sin(\varphi)\sin(\theta)|a_1\rangle - \cos(\theta)|s\rangle, \tag{B2}$$

two states with energies $E_\pm = \pm g$,

$$|\pm g\rangle = \frac{1}{\sqrt{2}}[\sin(\varphi)|e\rangle - \cos(\varphi)|r\rangle \pm \sin(\varphi)|a_0\rangle \mp \cos(\varphi)|a_1\rangle], \tag{B3}$$

and two states with energies $E_{\pm\lambda} = \pm\lambda$ with $\lambda = \sqrt{g^2 + \Omega_1^2 + \Omega_0^2}$,

$$|\pm\lambda\rangle = \frac{1}{\sqrt{2}}[\pm\cos(\varphi)|e\rangle + \sin(\theta)|s\rangle \pm \sin(\varphi)|r\rangle + \cos(\varphi)\cos(\theta)|a_0\rangle + \sin(\varphi)\cos(\theta)|a_1\rangle]. \tag{B4}$$

Here, the states $|a_j\rangle \equiv |g\rangle a_j^\dagger|0\rangle$ denote the states with one photon in mode a_j and all atoms in the ground state. The mixing angles are defined by

$$\tan(\varphi) = \frac{\Omega_0}{\Omega_1}, \quad \tan(\theta) = \frac{\sqrt{\Omega_1^2 + \Omega_0^2}}{g}. \tag{B5}$$

Note that due to the spatial dependence of the laser fields, the mixing angles vary with the distance to the origin which could violate the adiabaticity of the transition close to the cavity axis.

It is convenient to work in the adiabatic basis, where the loss of transfer efficiency due to the spontaneous decay shows up as population decay from the dark state. The probability amplitudes $\vec{A} = [a_g, a_{-g}, a_d, a_{-\lambda}, a_\lambda]^{\mathrm{T}}$ of the adiabatic states are connected to the diabatic amplitudes by the relation $\vec{A} = W\vec{B}$, where the orthogonal rotation matrix W is given by

$$W = \frac{1}{\sqrt{2}}\begin{bmatrix} \sin(\varphi) & 0 & -\cos(\varphi) & \sin(\varphi) & -\cos(\varphi) \\ \sin(\varphi) & 0 & -\cos(\varphi) & -\sin(\varphi) & \cos(\varphi) \\ 0 & -\sqrt{2}\cos(\theta) & 0 & \sqrt{2}\cos(\varphi)\sin(\theta) & \sqrt{2}\sin(\varphi)\sin(\theta) \\ -\cos(\varphi) & \sin(\theta) & -\sin(\varphi) & \cos(\varphi)\cos(\theta) & \sin(\varphi)\cos(\theta) \\ \cos(\varphi) & \sin(\theta) & \sin(\varphi) & \cos(\varphi)\cos(\theta) & \sin(\varphi)\cos(\theta) \end{bmatrix}. \tag{B6}$$

It is straightforward to show that the Schrödinger equation in the adiabatic basis reads $i\hbar\frac{d}{dt}\vec{A} = W^{-1}HW - iW\frac{d}{dt}W^{-1}\vec{A}$, where the last term describes the nonadiabatic transitions. As long as the spontaneous decay is sufficiently strong, the populations of the nonzero-energy adiabatic states change negligibly such that one can perform adiabatic elimination, $\dot{c}_{\pm g} = \dot{c}_{\pm\lambda} = 0$. Assuming $g \gg \frac{\dot{\varphi}^2}{\lambda}\cos(\theta)$ and neglecting terms of the order of $O(\dot{\varphi}^3)$, $O(\dot{\theta}^3)$, $O(\dot{\varphi}^2\dot{\theta})$, and $O(\dot{\varphi}\dot{\theta}^2)$, we find

$$P_{\mathrm{d}} \approx \exp\left\{-\frac{2\gamma}{g^2}\int_{-\infty}^{\infty}[\dot{\varphi}^2\sin^2(\theta) + \dot{\theta}^2\cos^2(\theta)]dt\right\}. \tag{B7}$$

One can evaluate the probability remaining in the adiabatic states during both stages of the protocol using the Rabi frequencies (18) and (19). We obtain $P_{\mathrm{d}}(\vec{r}) = e_a(\vec{r})$ with $a = 1, 2$, where

$$e_a(\vec{r}) = \exp\left\{-\frac{\gamma}{4T}\left(\frac{2}{g^2} - \frac{1}{g^2+\Omega^2} - \frac{1}{g^2+f_a^2\Omega^2}\right)\right\}. \tag{B8}$$

Here, $f_1 = \kappa_1(x)$ and $f_2 = x^2$.

APPENDIX C: FLUX INSERTION METHOD FOR NUMERICAL SIMULATION

Simulating the flux insertion protocol in Sec. III in the presence of particle-particle interactions is numerically challenging since it requires inclusion of all photonic modes as well as a large number of four-level atoms. In order to simplify the numerical integration, we replace the flux insertion technique based on STIRAP by another adiabatic transfer technique without coupling to an atomic medium. This protocol cannot directly be realized with the current cavity setup, but correctly captures the fidelity of the growing protocol for Laughlin states.

As before, we split the protocol into two steps:

$$\text{(i)}\ \ a_{3m} \to a_{3m+1}, \quad \text{(ii)}\ \ a_{3m+1} \to a_{3m+3}. \tag{C1}$$

To mimic the adiabatic transfer mediated by the atomic medium in an effective way, we add to the photonic Landau-level Hamiltonian, given by Eq. (1), a weak coupling between the lowest and first Landau level with time-dependent couplings,

$$H_c = \sum_m [g_a(t) a^\dagger_{3m} a_{3m+1} + g_b(t) a^\dagger_{3m+1} a_{3(m+1)} + \text{H.c.}]. \tag{C2}$$

The coupling $g_a(t)$ is on during step (i) and $g_b(t)$ during step (ii). Furthermore, $g_a, g_b \ll \Delta_{\text{LN}}$. We assume that the excited-state Landau-level energy can be changed linear in time t with respect to the lowest Landau-level energy,

$$\Delta(t) = -\Delta_0 + \frac{4\Delta_0}{\tau_\text{f}} \left| t - \frac{\tau_\text{f}}{2} \right|, \tag{C3}$$

where $\Delta_0 = \Delta_{0,1} - \Delta_{0,0}$. This resembles a rapid adiabatic passage protocol. Let us start with the adiabatic limit $t_\text{f} \to \infty$. In the first step, the coupling g_a is turned on and we transfer an OAM per photon of $1\hbar$ after the first step $t = t_\text{f}/2$. Then, g_a is turned off and g_b is turned on. The second step starts with detuning $\Delta(t_\text{f}/2) = -\Delta_0$ and transfers $2\hbar$ flux per photon to the system after time $t = t_\text{f}$. After a full step, we added three flux quanta per particle to the system. For adiabaticity, we require

$$\tau_\text{f} \gg \frac{4\Delta_0}{\Delta^2_{\text{LN}}}, \tag{C4}$$

which means that the detuning sweep $\Delta(t)$ must be slow compared to the many-body gap of the system.

[1] Z. Wang, Y. Chong, J. D. Joannopoulos, and M. Soljacic, Nature (London) **461**, 772 (2009).
[2] A. B. Khanikaev, S. Hossein Mousavi, W.-K. Tse, M. Kargarian, A. H. MacDonald, and G. Shvets, Nat. Mater. **12**, 233 (2013).
[3] M. C. Rechtsman, J. M. Zeuner, Y. Plotnik, Y. Lumer, D. Podolsky, F. Dreisow, S. Nolte, M. Segev, and A. Szameit, Nature (London) **496**, 196 (2013).
[4] M. Hafezi, E. Demler, M. Lukin, and J. Taylor, Nat. Phys. **7**, 907 (2011).
[5] C. Jörg, F. Letscher, M. Fleischhauer, and G. von Freymann, New J. Phys. **19**, 083003 (2017).
[6] J. Ningyuan, C. Owens, A. Sommer, D. Schuster, and J. Simon, Phys. Rev. X **5**, 021031 (2015).
[7] T. Peyronel, O. Firstenberg, Q.-Y. Liang, S. Hofferberth, A. V. Gorshkov, T. Pohl, M. D. Lukin, and V. Vuletic, Nature (London) **488**, 57 (2012).
[8] A. V. Gorshkov, J. Otterbach, M. Fleischhauer, T. Pohl, and M. D. Lukin, Phys. Rev. Lett. **107**, 133602 (2011).
[9] S. Baur, D. Tiarks, G. Rempe, and S. Dürr, Phys. Rev. Lett. **112**, 073901 (2014).
[10] I. Carusotto and C. Ciuti, Rev. Mod. Phys. **85**, 299 (2013).
[11] R. O. Umucalilar and I. Carusotto, Phys. Rev. Lett. **108**, 206809 (2012).
[12] M. Hafezi, A. S. Sorensen, E. Demler, and M. D. Lukin, Phys. Rev. A **76**, 023613 (2007).
[13] A. S. Sorensen, E. Demler, and M. D. Lukin, Phys. Rev. Lett. **94**, 086803 (2005).
[14] N. R. Cooper and N. K. Wilkin, Phys. Rev. B **60**, R16279(R) (1999).
[15] N. K. Wilkin and J. M. F. Gunn, Phys. Rev. Lett. **84**, 6 (2000).
[16] J. R. Abo-Shaeer, C. Raman, J. M. Vogels, and W. Ketterle, Science **292**, 476 (2001).
[17] V. Schweikhard, I. Coddington, P. Engels, V. P. Mogendorff, and E. A. Cornell, Phys. Rev. Lett. **92**, 040404 (2004).
[18] J. Otterbach, J. Ruseckas, R. G. Unanyan, G. Juzeliunas, and M. Fleischhauer, Phys. Rev. Lett. **104**, 033903 (2010).
[19] J. B. Götte, S. M. Barnett, and M. Padgett, Proc. R. Soc. London A **463**, 2185 (2007).
[20] N. Schine, A. Ryou, A. Gromov, A. Sommer, and J. Simon, Nature (London) **534**, 671 (2016).
[21] A. Sommer and J. Simon, New J. Phys. **18**, 035008 (2016).
[22] A. Sommer, H. P. Büchler, and J. Simon, arXiv:1506.00341.
[23] F. Grusdt, F. Letscher, M. Hafezi, and M. Fleischhauer, Phys. Rev. Lett. **113**, 155301 (2014).
[24] F. Letscher, F. Grusdt, and M. Fleischhauer, Phys. Rev. B **91**, 184302 (2015).
[25] S. Dutta and E. J. Mueller, Phys. Rev. A **97**, 033825 (2018).
[26] N. V. Vitanov, A. A. Rangelov, B. W. Shore, and K. Bergmann, Rev. Mod. Phys. **89**, 015006 (2017).
[27] J. D. Pritchard, D. Maxwell, A. Gauguet, K. J. Weatherill, M. P. A. Jones, and C. S. Adams, Phys. Rev. Lett. **105**, 193603 (2010).
[28] D. Petrosyan, J. Otterbach, and M. Fleischhauer, Phys. Rev. Lett. **107**, 213601 (2011).
[29] R. B. Laughlin, Phys. Rev. B **23**, 5632(R) (1981).
[30] M. F. Andersen, C. Ryu, P. Clade, V. Natarajan, A. Vaziri, K. Helmerson, and W. D. Phillips, Phys. Rev. Lett. **97**, 170406 (2006).
[31] M. Fleischhauer, A. Imamoglu, and J. P. Marangos, Rev. Mod. Phys. **77**, 633 (2005).
[32] J. Ningyuan, Al. Georgakopoulos, A. Ryou, N. Schine, A. Sommer, and J. Simon, Phys. Rev. A **93**, 041802(R) (2016).
[33] N. Jia, N. Schine, A. Georgakopoulos, A. Ryou, L. W. Clark, A. Sommer, and J. Simon, Nat. Phys. **14**, 550 (2018).
[34] F. Grusdt and M. Fleischhauer, Phys. Rev. A **87**, 043628 (2013).
[35] J. K. Jain, *Composite Fermions* (Cambridge University Press, Cambridge, 2007).
[36] Y.-H. Wu, H.-H. Tu, and G. J. Sreejith, Phys. Rev. A **96**, 033622 (2017).
[37] G. Moore and N. Read, Nucl. Phys. B **360**, 362 (1991).